Energy 336 (2025) 138413

Contents lists available at ScienceDirect

Energy

journal homepage: www.elsevier.com/locate/energy

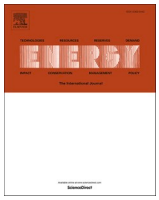

Experimental investigation on the effects of gliding arc plasma on the combustion characteristics of air stratified NH_3 flames

Ziyu Wang, B. Aravind *, Syed Mashruk, Agustin Valera-Medina

College of Physical Sciences and Engineering, Cardiff University, Wales, CF24 3AA, UK

ARTICLE INFO

Keywords:
Carbon-free fuel
Power generation
Net-zero
Nonequilibrium plasma
Flame morphology
Emission

ABSTRACT

This study investigates the impact of gliding arc plasma (GAP) on emission characteristics in NH_3-air flames with premixing ratios ranging from 0 % to 25 % at global equivalence ratios (ϕ) of 0.8 and 0.9. The experiments are carried out in a dual swirl burner, where a premixed NH_3-air mixture is introduced through the inner nozzle and central lance for GAP interaction, and non-premixed air is supplied via the outer nozzle. This study is the first to apply gliding arc plasma (GAP) to air-stratified ammonia flames, and this approach provides a significant and novel strategy for reducing NO_x emissions. The results show that GAP reduces NO_x emissions by up to 40 % under fully non-premixed conditions. At ϕ of 0.8, a critical transition appears when premixed air exceeds 20 %, resulting in increased NO emissions. In contrast, for $\phi = 0.9$, GAP consistently maintains stable NO reduction across all tested premixing ratios. The spectral analysis of the flame shows that the OH and NH_2 radicals play a pivotal role in mediating the effect of GAP on NO formation. These radicals exhibit competing influences, with NH_2 formation favoured under plasma activation. The NH_2 radical primarily forms through two plasma-driven pathways: $O(^2D) + NH_3 \rightarrow OH + NH_2$ and $N(^2D) + NH_3 \rightarrow NH + NH_2$. The observed reduction of NO with plasma is primarily due to the increased production of NH_2 related to OH.

1. Introduction

Ammonia (NH_3) is seeking high demand as a promising green fuel, due to its carbon-free combustion, substantial energy density and its economical storage requirements [1]. These attributes make it a compelling candidate to address the global energy crisis [2]. However, the poor combustion characteristics of pure NH_3 and the problem of high NO_x emissions still needs to be resolved [3,4]. To address these challenges, several strategies are commonly employed, including the co-firing of NH_3 with highly reactive fuels such as methane [5–7] and hydrogen [8–10], staged combustion [11], humidification [12], mild combustion [13] and plasma assisted combustion [14], among other techniques.

Considering the pronounced impact of kinetic and transport phenomena on the combustion enhancement, plasma assisted combustion (PAC) stands out as a pioneering combustion control strategy offering significant potential to improve ignition efficiency [15], optimize combustion performance [16,17] and reduce NO_x emissions [18]. While the positive effects of plasma are well-documented in hydrocarbon-based combustion, studies on its impact in ammonia combustion remain limited [15,19,20]. Choe et al. [18] demonstrated that nano-second repetitively pulsed discharges (NRP) can significantly reduce the NO_x emissions. To further investigate the promoting effect of NRP on ammonia-air flames, Sun et al. [21] analysed the flame formation process under NRP-induced conditions at the nanosecond scale. The studies on dielectric barrier discharge (DBD) assisted NH_3 combustion in premixed NH_3-H_2-air mixtures have shown that NO_x emissions increase with the application of plasma in both laminar and turbulent flames [22]. To elucidate the NO_x formation behaviour in DBD, Deng et al. [23] employed planar laser-induced fluorescence and chemiluminescence techniques to simultaneously analyse key intermediate radicals (NO/OH/NH_2). Their findings indicate that the primary increase in NO is attributed to the faster growth rate of OH radicals compared to that of NH_2 radicals. Sekiguchi [24] conducted an experimental study on PAC using microwave and suggested that the plasma power and gas flow rate significantly influence the NH_3 and N_2O concentrations. Jančauskas et al. [25] found that gliding arc plasma (GAP) assisted NH_3-air combustion increases the heat flux by 61 % at equivalence ratio (ϕ) of 0.83, shows the pronounced thermal effect. Lin et al. [26] investigated that the laminar combustion rate was significantly increased and could be

* Corresponding author.
E-mail address: balakrishnana4@cardiff.ac.uk (B. Aravind).

https://doi.org/10.1016/j.energy.2025.138413
Received 19 June 2025; Received in revised form 19 August 2025; Accepted 7 September 2025
Available online 9 September 2025

further improved by increasing the air flow rate in GAP. For NO_x emissions characteristics in GAP, Ju et al. [27] and Tang et al. [28] applied a gliding arc in combination with a cyclone burner and observed that GAP can significantly reduce NO emissions in premixed NH_3-air. Aravind et al. [29] demonstrated a significant reduction in NO emissions at lower plasma power by taking GAP and applying it to a non-premixed NH_3-air flame, where the plasma acted only on the NH_3 stream. Tang et al. [30] utilized NH-PLIF technology to demonstrate that plasma further extends the peak NH concentration to higher values. With plasma activation, the average peak NH concentration in the near-field region increased by >30 %. Apart from the aforementioned experimental studies on plasma-assisted combustion (PAC) of NH_3, several numerical investigations have also been conducted to better understand the underlying emission mechanisms. Taneja et al. [31] attributed the NO reduction with NRP to the deoxygenation and reduction processes of NO. These processes occur through several reaction pathways, including $NO + N \rightarrow N_2 + O$, $H_2 + NO \rightarrow H + HNO$, and $H_2 + NO \rightarrow NH + OH$. Mao et al. [32] investigated the effect of NO_x formation on ignition during NH_3-air combustion in DBD, showed that high concentrations of NO under lean conditions accelerated the generation of NNH and OH for maximum ignition enhancement.

Previous research has demonstrated that GAP is effective in enhancing flame stability and reducing NO production in both premixed and non-premixed NH_3-air flames [27,29]. Tu et al. [33] inferred that in non-premixed combustion, the OH intensity is significantly reduced as compared to premixed combustion in NH_3-CH_4-air flame. This diminished OH radicals impede the oxidation of NH_2 and NH radicals, thereby decelerating the formation of NO. Under identical gas flow conditions, the characteristics of NH_3-air flames differ significantly between non-premixed and premixed combustion systems, leading to distinct flame behaviours due to variations in flow field dynamics. Meanwhile, the stratified combustion facilitates control over local equivalence ratios via staged oxygen supply, thereby optimizing reaction pathways, enhancing fuel conversion efficiency, and improving thermal utilization. Its adaptability to variable fuel properties and complex flow configurations further supports its relevance to practical combustion applications [34]. Whether GAP exerts identical effects on both premixed and non-premixed combustion remains unclear, warranting further in-depth investigation. Consequently, the combustion-enhancing effect of GAP may exhibit corresponding modifications under these different combustion modes. Meanwhile, different gas components exhibit different properties when ionized, for instance air is more easily ionized than NH_3 [35]. Wang et al. [36] investigated the stability and NO emission behaviour during NH_3 stratification and air stratification in gliding arc plasma assisted combustion. Yu et al. [35] noted that at high energies, the electrical energy injected into the arc exceeds the energy loss due to turbulent dissipation, which puts GAP into glow mode. The electron energy in the glow mode discharge is not sufficient to completely dissociate NH_3, leading to the generation of intermediate products. The high energy consumption has different impact of GAP on combustion compared with lower power, and higher energy consumption is not expected.

In the present study, effect of GAP on the NO_x formation and flame topology of NH_3-air flame under air stratification is investigated. To understand the underlying mechanism of NO_x formation and consumption, the generated intermediate groups were analysed by spectral analysis. A numerical method is applied to investigate the generation of intermediate components in plasma and the effect of intermediate components on NO.

2. Materials and methods

2.1. Experimental apparatus

A novel plasma assisted dual-swirl burner developed at the Centre of Excellence on Ammonia Technologies (CEAT), Cardiff University is used to conduct the experiments. The schematic of the experimental setup is shown in Fig. 1. The experiment setup comprises of three components: the combustion unit, the plasma unit, and the diagnostic unit. In the combustion unit, the flow of NH_3 and air was controlled using high precision Alicat mass flow controller achieving an accuracy of ±0.5 % within 95 % of the full scale. Two radial co-swirlers having swirl numbers of 1.0 each [12] were positioned 125 mm and 40 mm from the dump plane for inner and outer swirlers. The NH_3 is introduced through the central lance via the inner swirler, while air flows through the outer swirler and exits at the dump plane. This configuration typically results in a non-premixed flame. Plasma is primarily generated within the annular gap between the central lance and a conical electrode, which also serves as a bluff body. To investigate the extent of premixing effects, a controlled fraction of air is added to the NH_3 stream. The flame is stabilized inside a quartz tube with a diameter of 58 mm and a height of 320 mm.

A high-voltage AC power supply (CTP-6 2000 KA, ACS Materials, USA) is used to generate the gliding arc plasma. The change in input plasma power was accomplished by adjusting the input voltage of the power supply. In this experiment, the input frequency was kept constant at 13 kHz, and the plasma input power was controlled to be between 100 and 110W (~1.6–1.8 % of the total combustion power) for the accurate comparison purpose. At the central lance of 16 mm diameter, a conical electrode made of tungsten-steel alloy with a maximum diameter of 11 mm was installed. A minimum electrode-to-wall gap of 2.5 mm was observed at breakdown. The arc was stretched upward by the gas flow until reaching its maximum length, after which it was blown out and the next breakdown followed.

The diagnostic system consisted of a digital camera, an oscilloscope, a spectrometer, a voltage probe, a current probe and a high-speed camera. The camera is set at 600 mm from the central plane of the burner. The camera maintained constant settings at f/4 aperture, exposure time of 1/3s, and ISO 64 throughout the photographic session. Voltage and current waveforms were captured using a Tektronix MSO64B oscilloscope connected to a Tektronix P6015 high-voltage probe and a Cybertek HCP 8030 current probe (5A, 1V/A). During the experiment, the input plasma power was calculated in real time based on the voltage and current curves to keep it constant. An AvaSpec-ULS spectrometer with a UV/visible optical fibre was set up 25 mm above the combustion chamber entrance [29]. At a working distance of 100 mm, the probe samples light from an area approximately 2–3 mm in diameter, providing localized spectral data within the 30 × 38 mm^2 measurement region. The chemiluminescence signals from OH ($A^2\Sigma^+$–$X^2\Pi$), NH* ($A^3\Pi$–$X^3\Sigma^-$), and NH_2* (NH_2 α band peak) were captured using bandpass filters: 309 nm (±10 nm FWHM), 336 nm (±10 nm FWHM), and 630 nm (±10 nm FWHM) [37]. For each condition, 200 frames were recorded with LaVision Davis v10, the intensity of chemiluminescence distribution is obtained by following three steps: time-averaged, subtracted the background and Abel transformed. For a given equivalence ratio and the same species, the intensity is normalized to the maximum intensity among the premixing cases, both with and without plasma. Therefore, it is not advisable to compare the chemiluminescence image among the different species with different equivalence ratios. The average grey value is calculated based on the average image of 200 images obtained by the high-speed camera with background correction. A gas analyser (Emerson CT5100 quantum cascade laser) was applied to derive exhaust emissions, including NO, NO_2, N_2O, NH_3, O_2, H_2O. Emissions were recorded at 1 Hz and subsequently averaged over a 2-min interval. Gas samples were collected using a 30 mm isokinetic sampling funnel positioned 15 mm downstream of the quartz tube exit. To prevent condensation, the sampling line was heated to and maintained at 463K. Data from 120 samples per test point were normalized to dry 15 % O_2. The experimental conditions controlled the constant combustion power of 6 kW (the corresponding flow rate of NH_3 of 26.9SLPM). In this study, experiments are performed for equivalence ratios of 0.8 and 0.9. At lean condition lower than 0.8, the flame was

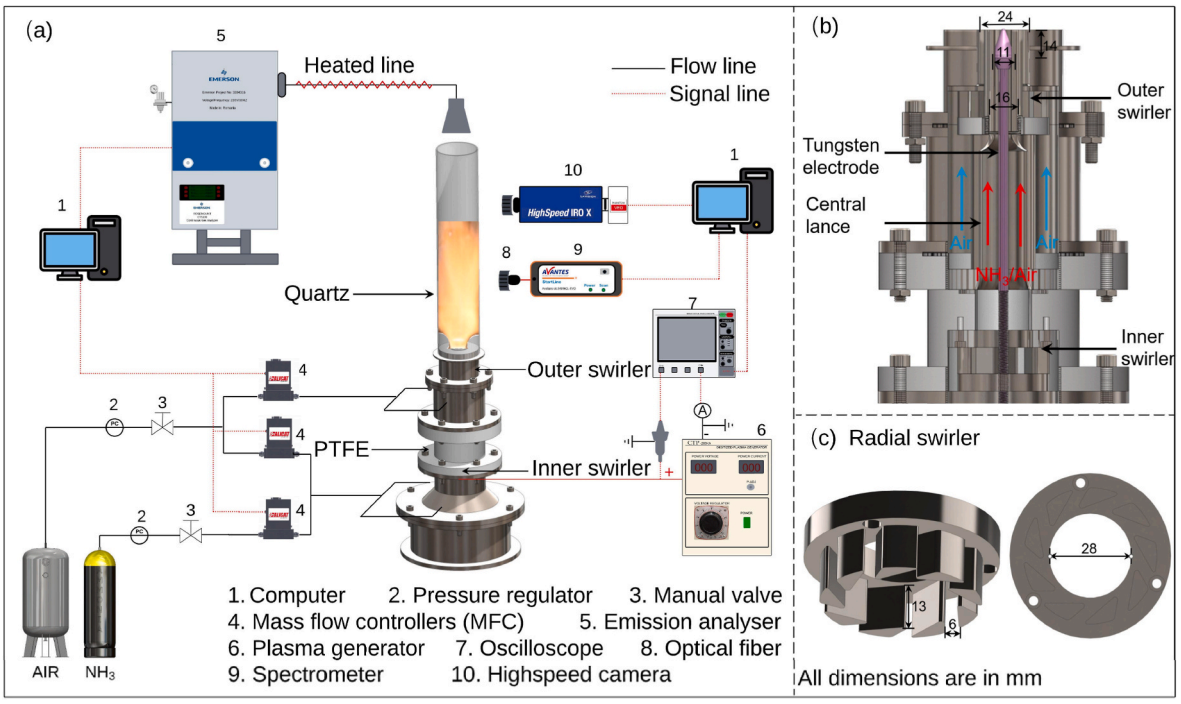

Fig. 1. Schematic of the experimental setup, (a) overall experiment setup, (b) details in burner, (c) radial swirler.

unstable in the absence of plasma action, resulting in the inability to obtain accurate emission measurement. In addition, in NH_3-air combustion, peak NO_x emissions typically occur in this range, therefore it is important to investigate the plasma effect in this range. The amount of premixed air within the mixture is 0–30 %. The premixing ratio (χ_{premix}) was calculated based on the total volume of the air in the reactant mixture. For example, zero premixing ratio is referred to as pure non-premixed NH_3-air mixture. As the flame appeared to start showing instability when the premixed gas reached 30 %, the emissions and spectrum were not recorded at that operating condition. The premixing ratio is calculated by the equation below:

$$\chi_{premix} = \frac{Q_{premixed\ air}}{(Q_{air})_{stoichiometric}/\phi} \quad (1)$$

Here Q represents the flow rate, SLPM. ϕ is the global equivalence ratio.

2.2. Electrical characteristics of GAP

The voltage-current characteristic curves at different χ_{premix} are shown in Fig. 3 in the same flow rate of NH_3 (Q_{NH3}).

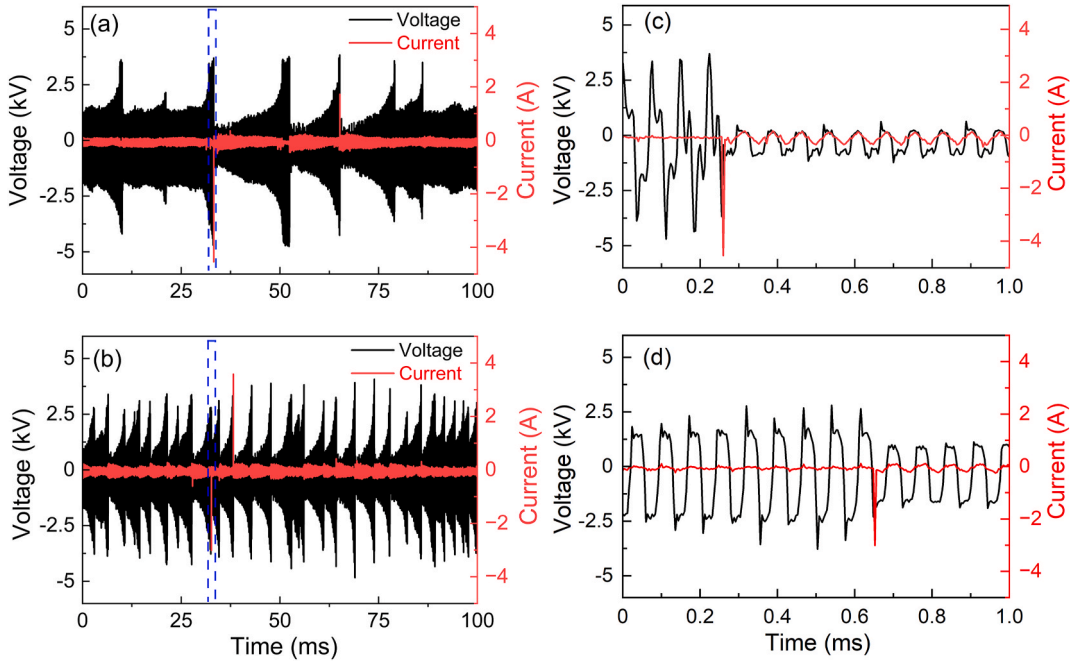

Fig. 2. Electrical characteristics of GAP at $\phi = 0.8$ for (a) $\chi_{premix} = 0$ %, 110W (b) $\chi_{premix} = 30$ %, 108W, (c) enlarged segment for $\chi_{premix} = 0$ %, (d) enlarged segment for $\chi_{premix} = 30$ %.

In GAP, the voltage and current show periodic variations [28]. The input power of the plasma can be determined from the measured voltage and current using the following equation [38]:

$$Power = \frac{1}{T}\int_0^t V \times Idt \quad (2)$$

In the experimental procedure, the plasma power was initially calibrated to fall within the required range of 100–110W. Following this, measurements including optical emission and chemiluminescence imaging were conducted. This approach ensured that the input power remained consistent across varying flow rates.

At the moment of breakdown, the current appears as a maximum value and a minimum value of voltage. Compared with Fig. 2(a) and (b), significant variations are in cycle time under approximately the same plasma power. With no premixed air (Q_{NH3} = 26.9SLPM), 8 cycles occur in 100 ms in Fig. 2 (a). For the 30 % premixed gas (Q_{NH3} = 26.9SLPM, Q_{air} = 36SLPM), 25 cycles occur in the same period in Fig. 2 (b). Simultaneously, the power injection at the moment of breakdown also varies considerably. The power at the breakdown moment in the glow-type phase is close to 0.8 kW in the absence of premixed gas and close to 1 kW in the 30 % premixed air condition. The variations in voltage and current characteristic curves within 1 ms are shown in Fig. 2(c) and (d). The extent of voltage drops before and after breakdown is illustrated. When χ_{premix} = 0 %, the voltage drops from 3.5 kV to 0.6 kV, while χ_{premix} = 30 %, it decreases from 2.5 kV to 1.5 kV. At the same plasma power, the gas flow in the tube is the main factor controlling the trend of voltage and current. When the gas flow increases, the arc is more prone to be blown out, then entering the next breakdown-stretching-extinguishing cycle. Concurrently the gas composition also influences the cycle period and electrical characteristic curve in GAP. As mentioned by Choi et al. [38], Higher hydrogen concentration is associated with shorter re-slip cycle and higher peak voltage.

2.3. Numerical methodology

To understand the underlying mechanism of GAP promotes the generation of intermediate groups, a numerical method coupling ZDPlaskin and Chemkin is used. The method is used extensively in theoretical analyses of plasma assisted NH_3 combustion [31,32,39,40]. The numerical methodology of the GAP simulation is similar to the work of Crispim et al. [41]. The computational region is divided into the ionization region and the external region. The distinction is based on the voltage-current characteristic curve. In the ionized region, there is a high electron density and therefore more active electronic reactions are present in this region. In the external region, on the other hand, it consists of reactions of more stable intermediate components. The plasma action mechanism and the plasma assisted mechanism of Mao et al. [32] were applied to this study.

3. Results and discussion

This study provides the first evidence that GAP can achieve a 40 % reduction in NO_x emissions in non-premixed ammonia flames, with the NH_2 radical pathway identified as a key mechanism contributing to this reduction.

3.1. Effect of plasma and air stratification on flame morphology

The effect of plasma and air stratification on flame morphology is shown in Fig. 3. These time averaged direct photographs were captured using a Nikon digital camera.

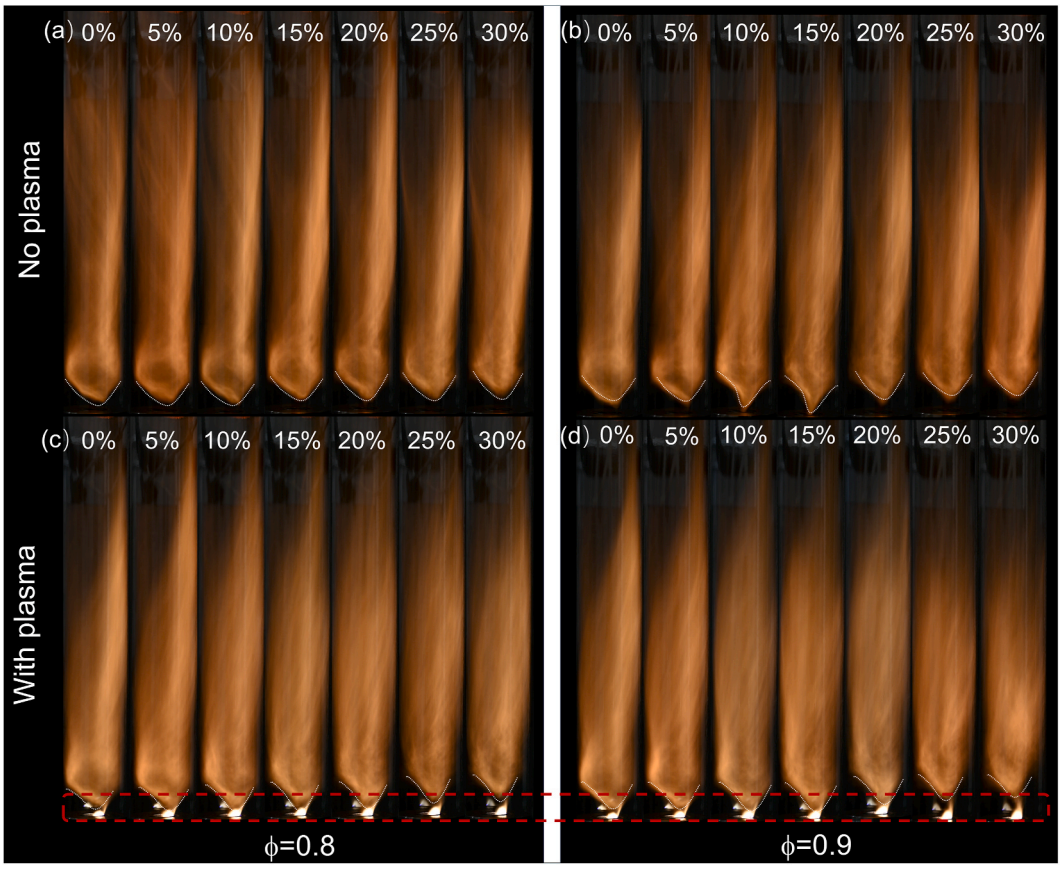

Fig. 3. Variation of flame morphology with different percentage of χ_{premix} from 0 to 30 % at no plasma ((a) ϕ = 0.8, (b) ϕ = 0.9) and plasma conditions ((c) ϕ = 0.8, (d) ϕ = 0.9).

Fig. 3 shows that all the flames exhibit a V-shaped structure, extending fully within the quartz tube irrespective of the operating conditions. For no plasma cases, in Fig. 3 (a) and 3(b), χ_{premix} below 5 %, the flame is either attached to the central lance or slightly lifted, with minimal influence from the bluff body. However, as the χ_{premix} increases, the flame increasingly tends to anchor to the conical bluff body due to the presence of premixed air. It is evident from Fig. 3(c) and (d) that plasma actuation has a strong impact on the flame anchoring. As emphasized by Ghabi et al. [42], the plasma significantly reduces the flame lift-off height for χ_{premix} from 0 % to 25 %, resulting in greater flame attachment to the bluff body as compared to the corresponding no plasma cases in Fig. 3(a) and (b) [25]. However, the flame becomes more unstable with plasma at χ_{premix} = 30 % cases, mainly due to changes in the plasma medium. In these cases, the flame starts to jump off, changing from a stable V-shape to tubular. At elevated premixing levels, plasma–air interactions intensify, leading to enhanced flame oscillations [27]. Enhanced oxygen ionization under plasma conditions reduces the local concentration of molecular oxygen compared to the plasma-free state, which in turn decreases the combustion rate relative to no plasma premixed gases [43]. This reduction in combustion intensity could be a potential reason for the observed deterioration in flame stability.

3.2. Effect of plasma and air stratification on emissions

The emissions characteristics of NO, NO_2, N_2O, and NH_3 for different premixed air ratios are shown in Figs. 4 and 5 for ϕ = 0.8 and 0.9 respectively to better illustrate the impact of plasma on emissions, Fig. 6 presents the percentage reduction of NO at different ϕ.

It can be seen from Fig. 4 (a), for ϕ = 0.8, NO concentration remains relatively constant at approximately 1200 ± 50 ppm up to a premixing level of = 15 %. Beyond this point, a noticeable increase is observed, reaching 1400 ppm at 30 %. Conversely, as shown in Fig. 5 (a) for ϕ = 0.9, the NO concentration is stable at 1100 ± 20 ppm up to χ_{premix} = 5 % followed by a sharp rise to 1500 ppm at χ_{premix} of 15 %. Interestingly, no significant change in NO levels is observed with further increases in χ_{premix} beyond this value. The comparative analysis of NO profile for Figs. 4 (a) and Fig. 5 (a) indicates that NO emissions are significantly lower under non-premixed conditions and tend to increase with higher levels of premixing. However, due to the limited premixing range examined in this study (up to 30 %), it is challenging to establish a definitive trend for NO behaviour at low premixing levels. This behaviour is closely linked to changes in flame structure and temperature, both of which play a critical role in governing NO formation and destruction pathways. A reduction in flame lift-off height, accompanied by modifications in flame morphology such as flame broadening, signifies an enlargement of the combustion reaction zone. This expansion contributes to a decrease in peak flame temperatures, thereby mitigating NO_X formation [33]. However, the trend between the two ϕ in the case of GAP assisted combustion demonstrates a notable difference. For instance, at ϕ = 0.9, plasma can reduce the NO to 400–1000 ppm irrespective of the premixing ratio. This corresponds to approximately 20 %. This is mainly attributed to the plasma action of NH_3 producing intermediate components such as NH_2, NH, as a potential reason for the decrease in NO. For ϕ = 0.8, at 0–15 % premixed gas ratios, GAP effectively reduces the production of NO as shown in Fig. 4 (a). Nevertheless, as the amount of premixed air increases further, the NO emission under GAP gradually caught up and even exceeded that under no GAP. In Fig. 6, This corresponds to the maximum NO reduction of 37 % at χ_{premix} = 0 % which gradually decreased to a 9 % reduction at χ_{premix} = 15 % for ϕ = 0.8. Excessive gas mixture flow reduces the residence time of the plasma and hinders the ionization effect [23]. Higher premixed air content also leads to the production of O atoms during ionization, which are converted to OH and promote the oxidation of NH_3 to NO [23]. Meanwhile, the increase of local OH radicals also significantly intensify the intensity of the local combustion reactions, resulting in localized zones of elevated temperature and energy [44]. This behaviour strongly depends on geometrical features of the burner such as gap length,

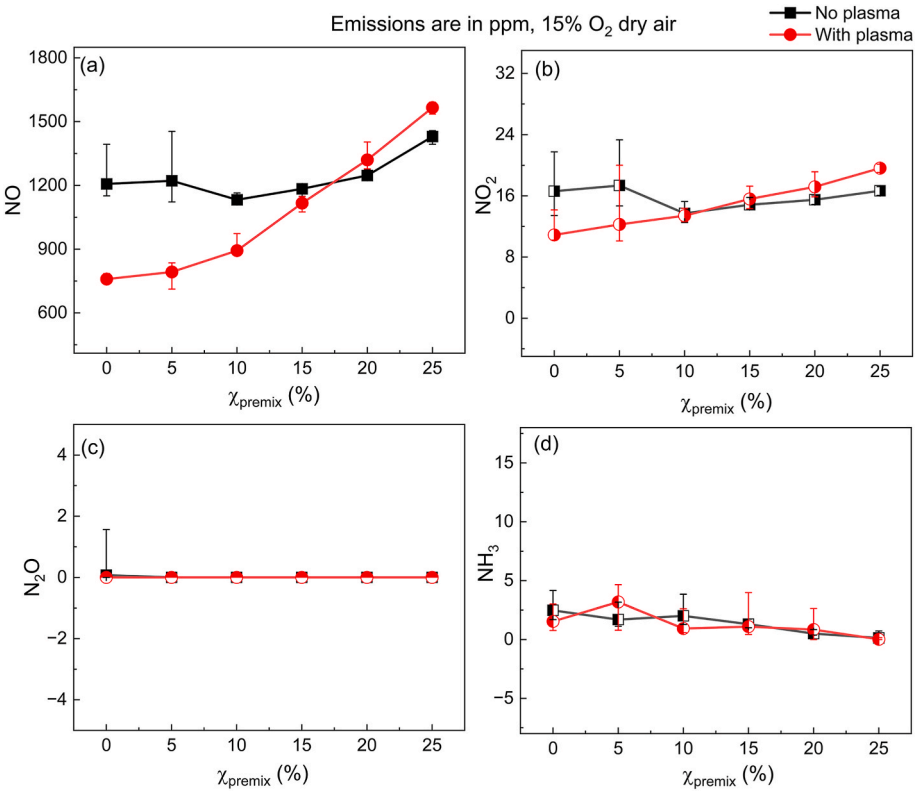

Fig. 4. The effect of plasma on the emission profiles of (a) NO, (b) NO_2, (c) N_2O and (d) NH_3 in different rates of χ_{premix} ranges from 0 to 25 % at ϕ = 0.8.

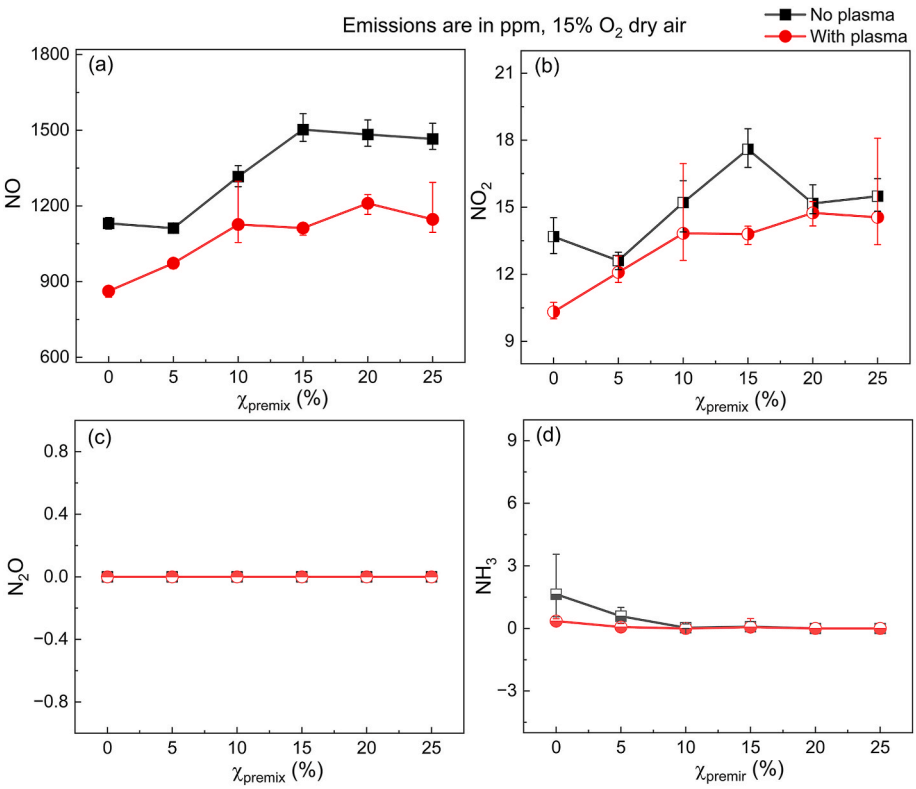

Fig. 5. The effect of plasma on the emission profiles of (a) NO, (b) NO_2, (c) N_2O and (d) NH_3 in different rates of χ_{premix} ranges from 0 to 25 % at $\phi = 0.9$.

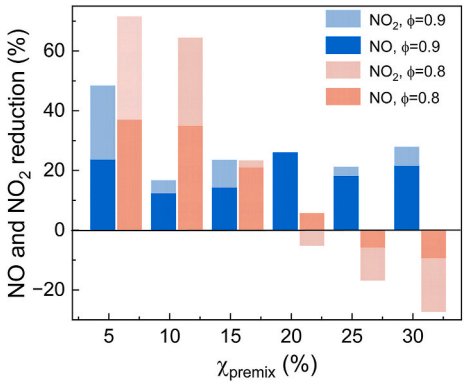

Fig. 6. NO reduction and NO_2 reduction in different premixed air with GAP. ($\phi = 0.8$ and 0.9, χ_{premix} = 0–25 %).

premixing lengths, diameter of electrode etc. and the plasma characteristics such as frequency, power, voltage etc. Therefore, a detailed parametric study is needed to identify the key parameters that influence the emission profile.

In the present study, NO_2 emissions vary between 10 and 20 ppm irrespective of the equivalence ratio and premixing ratio. The NO_2 profiles show a similar trend as that of the NO as shown in Figs. 4 (b) and Fig. 5 (b). This is mainly due to the production of NO_2 strongly depends on the $NO + HO_2 = NO_2 + OH$ reaction [45]. Li et al. [45] also pointed out that NO_2 primarily accumulates in low-temperature regions. For $\phi = 0.9$, NO_2 emissions are reduced by 0.6–3.7 ppm with plasma activation, corresponding to a 2 %–25 % decrease compared to the no plasma condition. While for $\phi = 0.8$, GAP reduces NO_2 emissions by up to 5.7 ppm (34 %) under non-premixed conditions. However, with increasing premixed air fraction, GAP may also lead to an increase in NO_2 emissions of up to 3 ppm (18 %). Since GAP generates thermal effects, which may elevate temperatures [46], this could further suppress NO_2 formation in low-temperature zones, thereby partially accounting for the NO_2 reduction observed in GAP. Furthermore, N_2O generation was not observed under all operating conditions, and NH_3 slip were always below 3 ppm in Fig. 4 (c) and 4 (d) and Fig. 5 (b) and 5 (d).

3.3. *Effect of plasma on the key intermediate species*

To understand the effect of key species due to the impact of plasma on the emission characteristic, simultaneous chemiluminescence imaging of NH_2* and OH* are captured for different χ_{premix} as shown in Fig. 7.

For NH_3 combustion, NH_2* is considered as a good heat release marker [25,28] and OH* can give indication about the NOx production pathways [23]. OH, can oxidize NH_2 or convert it into HNO, leading to an increase in NO. Meanwhile, the main NOx reduction reactions indicate that NH_2 is a key factor in suppressing NO formation [47]. A plasma mask is added to the imaging process to prevent image saturation. The NH_2* trace corresponds to the flame shape, with the highest intensity detected in the outer flame layer. An increase in the amount of premixed air monotonically attenuates the NH_2* and OH* signal strengths under no plasma action for all the equivalence ratios. In contrast, the change in signal strength is not monotonically variable under plasma action. The plasma significantly enhances the NH_2* and OH* signal strengths in all operating conditions, which is related to the presence of a considerable number of free radicals generated in the plasma ionization [48]. As shown in Fig. 4, the effect of plasma emission mitigation diminishes and begins to have a detrimental impact at a premixing ratio of 20 % for $\phi = 0.8$. This may be related to the increase in NH_2* and OH* shown in Fig. 7. The NH_2* and OH* groups show a competitive relationship in NO production [47], while the plasma promotes NH_2* production of 56.1 % and OH* production of 116.9 % at premixing ratio of 20 %, as it shown in Fig. 7(a) and (b). Plasma-induced reactions $e + NH_3 \rightarrow e + NH_2 + H$ and $O(^2D) + NH_3 \rightarrow OH + NH_2$ show that NH_3 can be converted into the free radical NH_2 [32]. The plasma-driven generation reactions of NH_2,

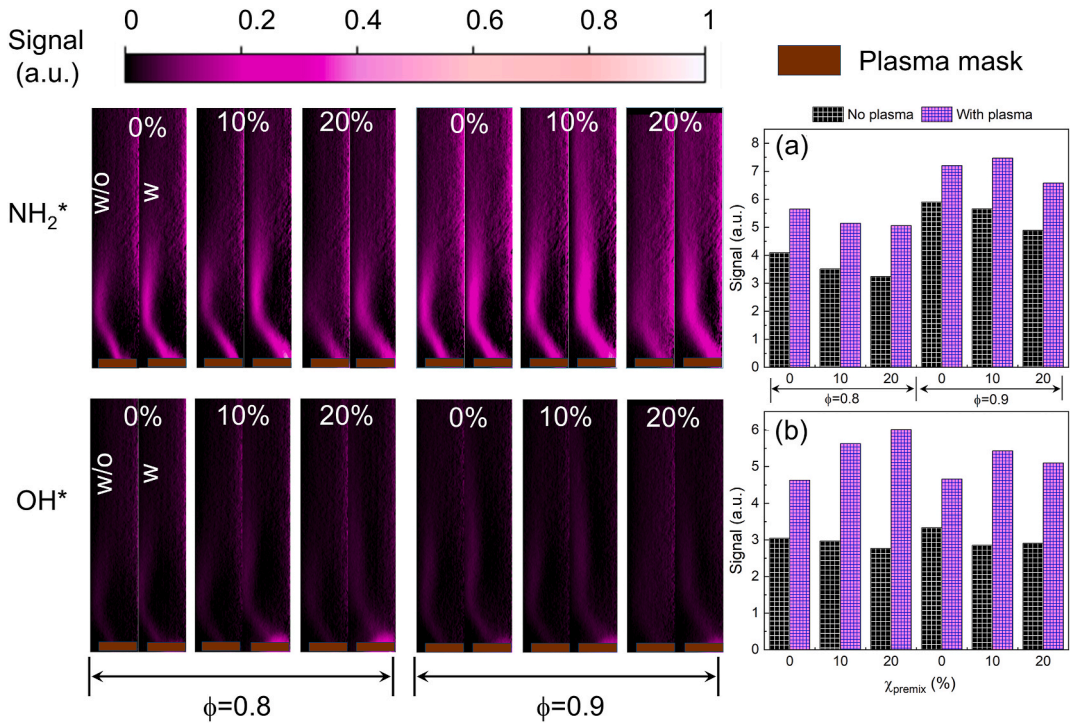

Fig. 7. Abel-deconvoluted OH* and NH_2* chemiluminescence images and average grey value of (a) NH_2*, (b) OH* in different χ_{premix} with GAP. (ϕ = 0.8 and 0.9, χ_{premix} = 0–20 %).

OH, and NH radicals are described in detail in Section 3.4. This may contribute to the increase of NO emission under plasma action. This phenomenon is attributed to the predominance of the air molecule in the gas mixture, leading to a relatively higher production of OH through HNO route [15]. This also explains the continued increase in NO emissions with the addition of premixed air after 20 % premixed air.

The spectral characteristics of NH_3-air flame under GAP in the wavelength range of 300 nm–900 nm for different χ_{premix} (0–20 %) and ϕ (0.8 and 0.9) are shown in Fig. 8.

As is shown in Fig. 8, the peaks occurred at 734 nm in all cases in NH_2 (α band, $^2A_1$-$^2B_1$) [28]. The signal from NH_2 (α-band, 2A1-2B1) occupies a dominant position throughout the visible wavelengths while showing a significant signal intensity [37]. And comparing the spectra with and without plasma, plasma can significantly enhance the intensity of this phase since NH_3 is decomposed in the plasma [49]. Fig. 9 (a) demonstrates that NH_2* experiences a 30–50 % magnitude increase at ϕ = 0.8. NH* exhibits more pronounced plasma-induced enhancement, achieving a peak intensity increase of 60 % at χ_{premix} = 10 %. Among the three radicals investigated, OH* exhibits the weakest plasma-induced enhancement, with an intensity increase of <10 % at ϕ = 0.9 in Fig. 9 (b). Although OH* enhancement promotes HNO formation and consequently elevates NO production, the net NO concentration ultimately decreases. This observation can be attributed to the substantially stronger enhancement of NH_2* and NH* radicals compared to OH*. Notably, plasma enhancement effects diminish when the premixed air fraction exceeds 25 %, as increased flow rates reduce plasma residence time, thereby weakening both thermal and kinetic effects of plasma activation.

3.4. *Mechanism of intermediate species generated in GAP*

The main generative sensitivities of the main intermediate groups

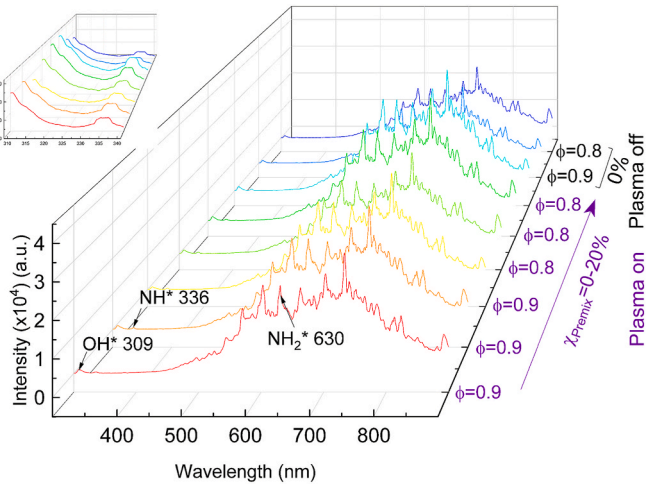

Fig. 8. Spectra of plasma assisted with NH_3-air flames. (ϕ = 0.8 and 0.9, χ_{premix} = 0–20 %).

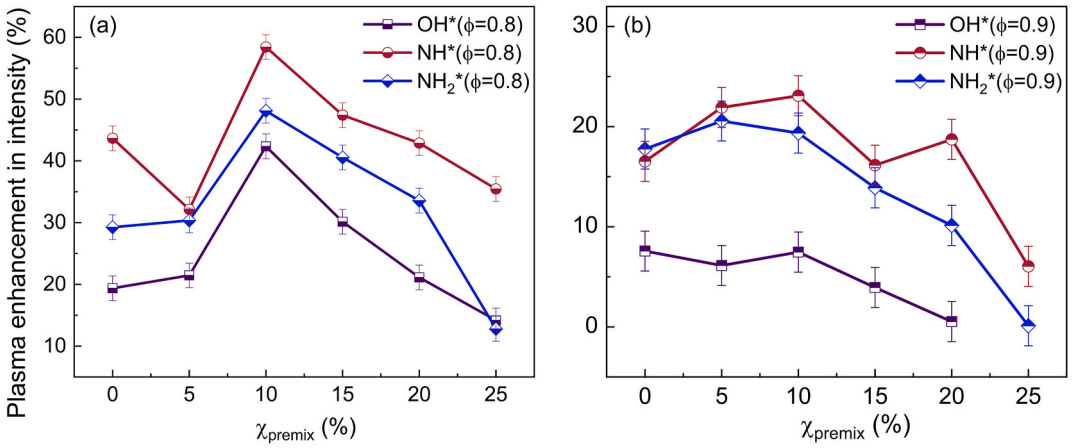

Fig. 9. Percentage enhancement of OH*, NH* and NH_2* chemiluminescence intensity in different rates of premixed air with GAP. (a) ϕ = 0.8, (b) ϕ = 0.9. (χ_{premix} = 0–25 %).

affecting NO (NH_2, NH, OH) in the plasma are analysed in Fig. 10. The purple region is the ionized region, and the white region is the outer region with no electron density.

In Fig. 10, major chemical reactions to produce NH_2, NH, OH in plasma were revealed. It can be observed that in the ionization phase, quenching of electronically excited $O(^1D)$, $O(^2D)$, $N(^2D)$ atoms are produced by electron impact dissociation [32]. They will undergo different dehydrogenation reactions with NH_3 to produce NH and NH_2. Among these, $O(^2D) + NH_3 = OH + NH_2$ presents the maximum rate of production. As suggested by Aravind et al. [19], the observed Lean Blowout (LBO) improvement likely results from plasma produced OH radicals that accelerate NH_3 breakdown and subsequently enhance flame propagation velocity. Simultaneously, in the initial phase, the reaction rates of different chemical pathways tend to decline, mainly as a result of the decreasing ionization rate of NH_3. When time enters the external phase, the electronic reaction stops, resulting in a rapid decrease of excited states of the nitrogen/oxygen atom, leading to a sudden decrease in the rate of intermediate group generation reactions, which eventually stabilizes at a low value. The different reaction rates also demonstrate that increasing the plasma residence time (5.64 ms in Fig. 10) dissociates with NH_3 increasing the generation of intermediate groups. However, as mentioned by Yu et al., the current observations of plasma dissociates NH_3 are qualitative rather than quantitative and more sophisticated diagnostics including electronic energy spectroscopy are needed to provide deeper insights [35].

The plasma assisted combustion and the sensitivity analysis of NO produced during combustion is shown in Fig. 11. The figure compares the amount of premixed air at 0 % and 10 %. The ten chemical reactions with the highest sensitivity of NO were selected and normalized separately.

Fig. 11 shows the sensitivity coefficients of NO emission for combustion reactions. The largest sensitivity of the production of NO is mainly through branched chain reactions of HNO: HNO + OH=NH_2+O, HNO + H=NH + OH. As mentioned by Elbaz et al. [50], HNO accounts for 70 % of NO formation, while N contributes only 10–15 % of the total NO production owing to the slower rate of N atom generation. NO is primarily generated through the reactions of NH_2, NH, and N radicals with O_2, O, OH, and HO_2, as well as via the intermediates HNO and H_2NO. Meanwhile, NH_2 and NH radicals primarily involved in NO reduction mainly forming N_2O, finally generating N_2 through reactions which are consumed by H atoms. NH_2 and NH groups play important roles in both generation and consumption in NO generation reactions [51]. Sabia indicated that within specific temperature and oxygen concentration ranges, thermal $DeNO_x$ reaction NH_2+NO=NNH + OH, NH_2+NO=N_2+H_2O play a dominant role and significantly influences flame speed prediction and NO_x formation [47]. Whereas these two consumed reactions present a greater sensitivity coefficient in the two plasma assisted combustion cases. Plasma can promote NO reduction perhaps attribute to $DeNO_x$ reactions of NH_2 and NH can be promoted at certain temperatures and oxygen concentration ranges. Since we have also observed that premixed air volumes up to 25 % with ϕ = 0.8, GAP conversely exacerbated the NO emissions. Nevertheless, the range of specific temperatures and oxygen concentrations is not clearly defined, and GAP affects both gas temperature and gas composition, thus it requires further study to find the range. Among the ten most sensitive

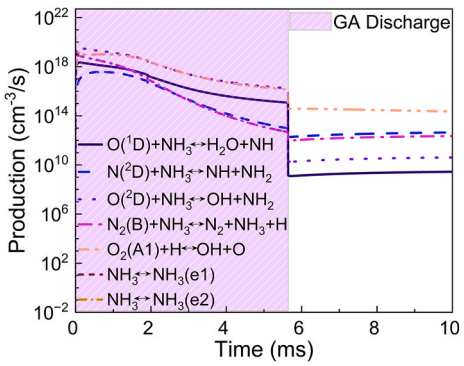

Fig. 10. Sensitivity analysis of intermediate species production in GAP of ϕ = 0.9, χ_{premix} = 10 %.

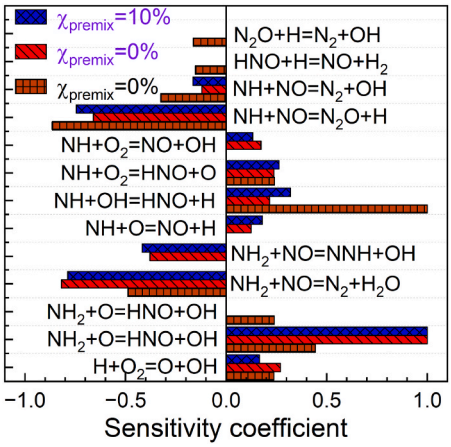

Fig. 11. Sensitivity analysis of NO emission. (ϕ = 0.9, with plasma (red and blue), no plasma (brown)).

reactions selected, no termolecular (three-body) reactions were involved, which may also reflect a limitation of the current mechanism and will need to be further improved in future work.

4. Conclusion

The impact of GAP on emissions from NH_3–air flame combustion under stratified air conditions is investigated. This study represents a significant step toward practical plasma-assisted ammonia combustion, particularly in terms of NO_x reduction, which contributes to the broader goal of decarbonization. The main conclusions summarised below.

1. The plasma decreases the flame lift-off height of χ_{premix} from 0 % to 25 %, enhancing flame attachment to the bluff body compared to no plasma cases. However, as the χ_{premix} up to 30 %, plasma introduction increases flame instability. Elevated oxygen ionization under plasma further depletes local O_2 concentrations, thereby reducing combustion rates relative to plasma-free premixed conditions.
2. The variations in OH* and NH_2* chemiluminescence may elucidate the influence of GAP on NO formation mechanisms. Under conditions where GAP reduces NO emissions, the plasma consistently promotes higher NH_2*/OH* generation ratios. The enhanced NO generation by plasma at $\phi = 0.8$, $\chi_{premix} = 20$ % is potentially associated with the more pronounced increase in OH* (116.9 %) radicals relative to NH_2* (56.1 %).
3. NO emission could be consumed through these pathways: $NH_2 + NO \rightarrow NNH + OH$, $NH_2 + NO \rightarrow N_2 + H_2O$. Meanwhile, NH_2 radicals, responsible for NO consumption, are mainly produced via these two reaction pathways under plasma conditions: $O(^2D) + NH_3 = OH + NH_2$, $N(^2D) + NH_3 = NH + NH_2$.

Diagnostic approaches focusing solely on NH_2* and OH* chemiluminescence could be insufficient, as the plasma's influence on flame propagation and compositional changes requires further investigation.

CRediT authorship contribution statement

Ziyu Wang: Writing – original draft, Methodology, Investigation, Formal analysis, Data curation. **B. Aravind:** Writing – review & editing, Supervision, Methodology, Investigation, Funding acquisition, Formal analysis, Data curation, Conceptualization. **Syed Mashruk:** Writing – review & editing, Resources. **Agustin Valera-Medina:** Writing – review & editing, Supervision, Resources, Funding acquisition.

Declaration of competing interest

The authors declare that they have no known competing financial interests or personal relationships that could have appeared to influence the work reported in this paper.

Acknowledgements

This work was supported by the European Union Project CAIPIRI-NH3A, under the GA Number 101191768. Views and opinions expressed are however those of the author(s) only and do not necessarily reflect those of the European Union or CINEA. Neither the European Union nor the granting authority can be held responsible for them. The research was undertaken at Cardiff University's Thermofluids Lab (W/0.17) with invaluable technical support from Mr. Jonathan Martin. For the purpose of open access, the author has applied a CC BY copyright licence to any Author Accepted Manuscript version arising. Information on the data underpinning this publication, including access details, can be found in the Cardiff University Research Data Repository at https://doi.org/10.17035/cardiff.29617334.v1.

Data availability

Data will be made available on request.

References

[1] Jafar U, Nuhu U, Khan WU, Hossain MM. A review on green ammonia as a potential CO_2 free fuel. Int J Hydrogen Energy 2024;71:857–76.
[2] Valera-Medina A, Xiao H, Owen-Jones M, David WIF, Bowen PJ. Ammonia for power. Prog Energy Combust Sci 2018;69:63–102.
[3] Hayakawa A, Arakawa Y, Mimoto R, Somarathne KDKA, Kudo T, Kobayashi H. Experimental investigation of stabilization and emission characteristics of ammonia/air premixed flames in a swirl combustor. Int J Hydrogen Energy 2017;42(19):14010–8.
[4] Mashruk S, Shi H, Mazzotta L, Ustun CE, Aravind B, Meloni R, et al. Perspectives on NO_X emissions and impacts from ammonia combustion processes. Energy Fuels 2024;38(20):19253–92.
[5] Valera-Medina A, Marsh R, Runyon J, Pugh D, Beasley P, Hughes T, et al. Ammonia–methane combustion in tangential swirl burners for gas turbine power generation. Appl Energy 2017;185:1362–71.
[6] Okafor EC, Somarathne KDKA, Ratthanan R, Hayakawa A, Kudo T, Kurata O, et al. Control of NO_x and other emissions in micro gas turbine combustors fuelled with mixtures of methane and ammonia. Combust Flame 2020;211:406–16.
[7] Xiao H, Valera-Medina A, Bowen PJ. Study on premixed combustion characteristics of co-firing ammonia/methane fuels. Energy 2017;140:125–35.
[8] Khateeb AA, Guiberti TF, Zhu X, Younes M, Jamal A, Roberts WL. Stability limits and NO emissions of technically-premixed ammonia-hydrogen-nitrogen-air swirl flames. Int J Hydrogen Energy 2020;45(41):22008–18.
[9] Mashruk S, Kovaleva M, Alnasif A, Chong CT, Hayakawa A, Okafor EC, et al. Nitrogen oxide emissions analyses in ammonia/hydrogen/air premixed swirling flames. Energy 2022;260:125183.
[10] Shi H, Liu Z, Mashruk S, Alnajideen M, Alnasif A, Liu J, et al. Modeling and optimization of ammonia/hydrogen/air premixed swirling flames for NO_x emission control: a hybrid machine learning strategy. Energy 2025;330:136735.
[11] Yamashita H, Hayakawa A, Okafor EC, Colson S, Somarathne KDKA, Tsujimura T, et al. Optimum primary equivalence ratio for rich-lean two-stage combustion of non-premixed ammonia/methane/air and ammonia/hydrogen/air flames in a swirling flow. Fuel 2024;368:131598.
[12] Davies J, Mashruk S, Sato D, Mazzotta L, Pugh D, Valera-Medina A. Emissions analyses of humidified cracked ammonia swirling flames. Combust Flame 2025;274:113984.
[13] Jiang T, Dai L, Zou C, Li W, Shi H, Yu Y. Ammonia/syngas MILD combustion by a novel burner. Combust Flame 2023;256:112943.
[14] Ju Y, Sun W. Plasma assisted combustion: dynamics and chemistry. Prog Energy Combust Sci 2015;48:21–83.
[15] Shah ZA, Mehdi G, Congedo PM, Mazzeo D, De Giorgi MG. A review of recent studies and emerging trends in plasma-assisted combustion of ammonia as an effective hydrogen carrier. Int J Hydrogen Energy 2024;51:354–74.
[16] Ju Y, Lefkowitz JK, Reuter CB, Won SH, Yang X, Yang S, et al. Plasma assisted low temperature combustion. Plasma Chem Plasma Process 2016;36(1):85–105.
[17] Ghabi A, Darny T, Dozias S, Escot Bocanegra P, Pouvesle J-M, Sarh B, et al. Effects of pulsed gliding arc plasma on non-premixed CH4/CO2– air flame stability. Therm Sci Eng Prog 2023;40:101764.
[18] Choe J, Sun W, Ombrello T, Carter C. Plasma assisted ammonia combustion: simultaneous NO_x reduction and flame enhancement. Combust Flame 2021;228:430–2.
[19] Aravind B, Yu L, Lacoste D. Enhancement of lean blowout limits of swirl stabilized NH_3-CH_4-Air flames using nanosecond repetitively pulsed discharges at elevated pressures. Applications in Energy and Combustion Science 2023;16:100225.
[20] Aravind B, Yu L, Lacoste DA. Understanding the coupling between nanosecond repetitively pulsed discharges and the thermoacoustic behavior of a swirl flame at 2 bar. Proc Combust Inst 2024;40(1):105211.
[21] Sun J, Bao Y, Zhang K, Konnov AA, Richter M, Kristensson E, et al. A comprehensive study on dynamics of flames in a nanosecond pulsed discharge. Part II: Plasma-assisted ammonia and methane combustion. Combust Flame 2025;275:114076.
[22] Ju R, Wang J, Zhang M, Mu H, Wu Y, Zhang G, et al. Experimental study on burning velocity, structure, and NO_x emission of premixed laminar and swirl NH_3/H_2/air flames assisted by non-thermal plasma. Applications in Energy and Combustion Science 2023;14:100149.
[23] Deng K, He A, Ye S, Lin W, Kang W, Lin Q, et al. Addressing NO_X formation mechanisms of NH_3/H_2 dual-fuel flame under DBD plasma-assisted combustion resolved by intermediate radicals analysis. Int J Hydrogen Energy 2024;96:938–51.
[24] Sekiguchi H. Experimental investigations of plasma-assisted ammonia combustion using rod-electrode-type microwave plasma source. Int J Hydrogen Energy 2024;65:66–73.
[25] Jančauskas A, Paulauskas R, Bykov E, Zakarauskas K, Ambrazevičius I. Gliding arc plasma effect on thermal characteristics of ammonia/biogas flames. Therm Sci Eng Prog 2025;60:103494.
[26] Lin Q, Jiang Y, Liu C, Chen L, Zhang W, Ding J, et al. Controllable NO emission and high flame performance of ammonia combustion assisted by non-equilibrium plasma. Fuel 2022;319:123818.

[27] Ju R, Wang J, Zhang M, Mu H, Zhang G, Yu J, et al. Stability and emission characteristics of ammonia/air premixed swirling flames with rotating gliding arc discharge plasma. Energy 2023;277:127649.
[28] Tang Y, Xie D, Shi B, Wang N, Li S. Flammability enhancement of swirling ammonia/air combustion using AC powered gliding arc discharges. Fuel 2022;313:122674.
[29] Aravind B, Wang Ziyu, Mashruk Syed, Lacoste Deanna A, Valera-Medina A. Novel strategy for combustion enhancement of NH_3-air mixture using gliding arc plasma. Proc Combust Inst 2025;41.
[30] Tang H, Gubbi S, Sun W. Investigation of flame structure in plasma-assisted ammonia swirling flames using NH planar laser-induced fluorescence. Combust Flame 2025;274:114006.
[31] Taneja TS, Johnson PN, Yang S. Nanosecond pulsed plasma assisted combustion of ammonia-air mixtures: effects on ignition delays and NO_x emission. Combust Flame 2022;245:112327.
[32] Mao X, Zhong H, Liu N, Wang Z, Ju Y. Ignition enhancement and NOx formation of NH_3/air mixtures by non-equilibrium plasma discharge. Combust Flame 2024;259:113140.
[33] Tu Y, Xu S, Liu H. Combustion and emission characteristics of NH_3/CH_4/air in a model swirl combustor: comparison between premixed and non-premixed modes. Int J Hydrogen Energy 2023;48(45):17311–23.
[34] Liu Z, Tu Y, Zhang H, Liu H, Luo Z, Zhang S, et al. Large eddy simulation study on the effects of swirl number on dynamic combustion characteristics of stratified methane swirling flame. Energy 2025;333:137458.
[35] Yu T, Zhang H, Zhao Z, Kong C, Zhang R, Zhu J, et al. Characteristics of an AC rotating gliding arc discharge in NH_3 and air atmospheres. Phys Plasmas 2024;31(2).
[36] Wang S, Wei X, Gu M, Lin Q, Luo G, Hu F. Flame characteristics and NO emission law of sliding arc plasma-assisted ammonia combustion. Combust Flame 2025;274:114000.
[37] Gaydon A. The spectroscopy of flames. springer science & business media; 2012.
[38] Choi J, Choi S, Song Y-H, Lee DH. Characterization of gliding arc discharge using H_2/Ar gas mixture. Int J Hydrogen Energy 2025;106:888–95.
[39] Shahsavari M, Konnov AA, Bai X-S, Valera-Medina A, Li T, Jangi M. Synergistic effects of nanosecond plasma discharge and hydrogen on ammonia combustion. Fuel 2023;348:128475.
[40] Zhong H, Mao X, Liu N, Wang Z, Ombrello T, Ju Y. Understanding non-equilibrium N_2O/NO_x chemistry in plasma-assisted low-temperature NH_3 oxidation. Combust Flame 2023;256:112948.
[41] Crispim LWS, Hallak PH, Benilov MS, Ballester MY. Modelling spark-plug discharge in dry air. Combust Flame 2018;198:81–8.
[42] Ghabi A, Boushaki T, Escot Bocanegra P, Robert E. Laminar burning velocity, adiabatic flame temperature, and pollutants of biogas/air mixture at various CO2 concentrations and plasma assist. Combust Sci Technol 2023;195(7):1599–621.
[43] Srinivasarao M, Kumar S, Jik Lee B, Giri BR, Shrestha KP, Mahendra Reddy V. Experimental and numerical analysis on influence of air staging in a tangential flow burner for pure ammonia combustion. Appl Therm Eng 2025;266:125580.
[44] Liang J, Chen M, Li K, Cheng C, Meng X, Gu M, et al. Discharge and emission characteristics of rotating gliding arc plasma using air, ammonia, and ammonia/air mixtures. Plasma Sci Technol 2025;27(7):075401.
[45] Li R, Konnov AA, He G, Qin F, Zhang D. Chemical mechanism development and reduction for combustion of $NH_3/H_2/CH_4$ mixtures. Fuel 2019;257:116059.
[46] Dong G, Zhou Y, Ming P, Wu Z, Chen H, Huang Y, et al. Kinetics-based analysis of the gliding arc plasma assisted ammonia decomposition process towards vehicle on-board applications. Chem Eng J 2025;505:159443.
[47] Sabia P, Manna MV, Cavaliere A, Ragucci R, de Joannon M. Ammonia oxidation features in a jet stirred flow reactor. The role of NH_2 chemistry. Fuel 2020;276:118054.
[48] Shahed Gharahshiran V, Zheng Y. Sustainable ammonia synthesis: an in-depth review of non-thermal plasma technologies. J Energy Chem 2024;96:1–38.
[49] Zheng Z, Wang C, Xin Z, Hu Y, Zhu Q, Yang W, et al. Kinetic modelling of non-equilibrium plasma enhanced catalytic ammonia decomposition. J Energy Inst 2024;116:101715.
[50] Elbaz AM, Wang S, Guiberti TF, Roberts WL. Review on the recent advances on ammonia combustion from the fundamentals to the applications. Fuel Communications 2022;10:100053.
[51] Zhang M, Wei X, An Z, Okafor EC, Guiberti TF, Wang J, et al. Flame stabilization and emission characteristics of ammonia combustion in lab-scale gas turbine combustors: recent progress and prospects. Prog Energy Combust Sci 2025;106:101193.